ELSEVIER

Catalysis Today 38 (1997) 47–58

CATALYSIS TODAY

Modeling and simulation of SO_2 oxidation in a fixed-bed reactor with periodic flow reversal

Ruoyu Hong[a,*], Xin Li[a], Hongzhong Li[a], Weikang Yuan[b]

[a]*Multiphase Reaction Laboratory, Institute of Chemical Metallurgy, Chinese Academy of Sciences, P.O. Box 353, Beijing 100080, China*
[b]*UNILAB Research Center of Chemical Reaction Engineering, East China University of Science and Technology, Shanghai 200237, China*

Abstract

The fixed-bed catalytic reactors with periodic flow-reversal operation are used to oxidize sulfur dioxide, specially that in the exhausted gas from the non-ferrous metal industry. A one-dimensional two-phase unsteady-state model describing this reactor is derived carefully from the mass conservation of sulfur dioxide and the heat for each phase. The Crank–Nicolson predictor–corrector method on a non-uniform spatial grid is used in solving the derived partial differential equations. The prime feature of the numerical method is that it is of the second-order accuracy both in time and in space. The two-way linked list is selected to store the temperature and concentration in the node points for adapting the change of the node number. Thus the computation accuracy and speed are improved remarkably. Numerical simulation of sulfur dioxide oxidation over vanadium catalysts in a small reactor is presented as an example. Numerical results showed that autothermal oxidation of low concentration sulfur dioxide is feasible. The results are compared with experimental data. The parameter sensitivity is carried out carefully for the mathematical model. Different influences (bed length, gas velocity of bed, initial bed temperature, feed concentration and cycle time) on maximum gas temperature and average conversion, etc., are obtained.

Keywords: Sulfur dioxide; Oxidation; Fixed-bed reactor; Flow-reversal operation; Simulation

1. Introduction

Sulfuric acid is an important chemical in great demand in industry. In the conventional process for conversion of SO_2 on vanadium catalysts, cold inlet gas must be preheated to a certain temperature before being fed into the first-stage reactor. Huge and costly heat exchangers are needed to keep the catalyst efficiency high and prevent the catalysts from sintering. Therefore, such a process is characterized with large investment and intrinsic difficulty in operation.

In most cases, the tail gas with a SO_2 concentration lower than 5% is produced in non-ferrous metallurgical processes. The conventional multiple-stage adiabatic reactors have difficulty in disposing this kind of gas.

There are two ways for innovating this kind of reactor. One is to develop new kinds of catalysts with high activity at high temperature (this belongs to the catalyst engineering). The other is to invent new catalytic reactors (this belongs to the reactor engineering). In recent years, great progress has been made in the latter field.

The major advantages of the fixed-bed catalytic reactors with periodic flow reversal over the conven-

*Corresponding author. Tel.: (86-10) 6255-4678; Fax: (86-10) 6256-1822; e-mail: hry@ccastb.ccast.ac.cn

PII S0920-5861(97)00038-2

tional multistage adiabatic ones are the elimination of interstage tubular heat exchangers and the possibility of treating cold inlet gas with low concentration of sulfur dioxide. Thus SO_2 in exhausted gas in the nonferrous metal industry is oxidized in the fixed-bed catalytic reactors with periodic flow reversal recently.

Matros [1,2] successfully invented a fixed-bed reactor with periodic flow reversal for oxidizing SO_2. Compared with the conventional ones, the interstage heat exchangers are removed, the requirements for process control are relaxed and the pressure drop of the system is reduced. Meanwhile, it could work smoothly when the SO_2 concentration of inlet gas is lower than 5% and is free of the interferences of temperature fluctuation, flow rate and feed concentration of SO_2. In order to optimize the design and operation, numerical simulation is a necessary tool. Matros [3] used a one-dimensional heterogeneous unsteady-state model wherein the transient terms in the mass conservation equations of both phases were neglected, with error introduced inevitably. He used a classic explicit method to solve the equations, which was time-consuming and sometimes unstable. Eigenberger [4] examined the effects of model parameters. But he employed a one-dimensional pseudo-homogeneous model, which had low credibility. He solved the model equations using a finite difference method with non-equidistance spatial steps [5].

In this paper, the model equations are carefully derived based on the previous research work, and solved with a new numerical method. A numerical example is presented and the results are compared with the experimental data. The parameter sensitivity is carried out carefully. Different influences on temperature profile and conversion, etc., are obtained.

2. The fixed-bed catalyst reactor with periodic flow reversal

A schematic flowsheet of the fixed-bed reactor with flow-reversal operation is illustrated in Fig. 1. Before cold inlet gas is fed, the catalytic bed is preheated to a certain high temperature (above ignition temperature). Then the cold inlet gas with low concentration of SO_2 is fed into the reactor. In the region near the entrance, the temperature of cold gas rises gradually while flowing forward, because the gas is heated by the hot solid particles. When the gas temperature exceeds the ignition temperature, the oxidation reaction of SO_2 occurs. The gas temperature rises rapidly and may be higher than the solid temperature. Therefore, the solid particles at relatively low temperature are heated by the hot gas near the exit of the reactor. It can be seen that the catalyst bed can be divided into three regions: the reaction zone in the center, wherein chemical reactions take place, and the two zones at the two ends of the reactor, which serve as heat exchangers.

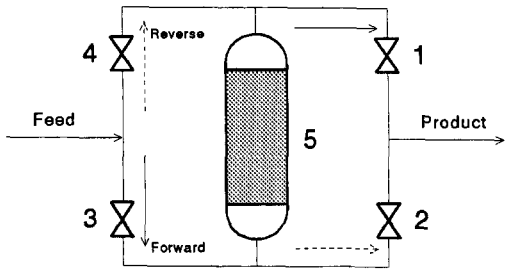

Fig. 1. Schematic flowsheet of the fixed-bed reactor with flow-reversal operation (1–4, valve; 5, fixed-bed reactor).

3. Model equations, boundary and initial conditions

3.1. *Derivation of model equations and model characteristics*

In a fixed-bed reactor with periodical flow reversal, the heat transfer between gas and particle phases is the most important, because the cold inlet gas has to be heated by the hot solids near the entrance of the reactor and the cold solids heated by hot gas near the exit of the reactor in order to eliminate preheating of inlet gas. Thus, the temperature and concentration differences between the gas and particle phases are accounted. The following assumptions are adopted before deriving the model equations:

1. The temperature and concentration gradients inside a catalyst pellet are negligible.
2. The flow is one-dimensional, the radial heat and mass gradients can be neglected, and the backmixing of the gas in the fixed-bed reactor can be modeled with axial dispersion.

3. The axial heat conduction of reactor wall can be neglected.
4. Not only the gas phase but also the particle phase can be assumed as continuum medium.

3.1.1. The model equations

The four equations, which are derived carefully in [21], are given as follows:

The concentration equation for the gas phase:

$$\frac{\partial C_f}{\partial t} + U \cdot \frac{\partial C_f}{\partial X} = A1 \cdot \frac{\partial^2 C_f}{\partial X^2} + A2 \cdot (C_c - C_f). \quad (1)$$

The temperature equation for the gas phase:

$$\frac{\partial T_f}{\partial t} + U \cdot \frac{\partial T_f}{\partial X} = A3 \cdot \frac{\partial^2 T_f}{\partial X^2} + A4 \cdot (T_c - T_f) + A5 \cdot (T_w - T_f). \quad (2)$$

The concentration equation for the particle phase:

$$\frac{\partial C_c}{\partial t} = A6 \cdot (C_f - C_c) - r(C_c, T_c). \quad (3)$$

The temperature equation for the particle phase:

$$\frac{\partial T_c}{\partial t} = A7 \cdot \frac{\partial^2 T_c}{\partial X^2} + A8 \cdot r(C_c, T_c) + A9 \cdot (T_f - T_c) + A10 \cdot (T_w - T_f) \quad (4)$$

with the parameters:

$$A1 = D_{ea}, \quad A2 = \frac{(1-\epsilon) \cdot a_v \cdot \beta}{\epsilon}, \quad A3 = \frac{\lambda_{ef}}{\rho_f \cdot C_{pf}},$$

$$A4 = \frac{(1-\epsilon) \cdot a_v \cdot \alpha_{fc}}{\epsilon \cdot \rho_f \cdot C_{pf}}, \quad A5 = \frac{2 \cdot \alpha_{fw}}{R \cdot \rho_f \cdot C_{pf}},$$

$$A6 = a_v \cdot \beta, \quad A7 = \frac{\lambda_{ec}}{\rho_c \cdot C_{pc}}, \quad A8 = \frac{(-\Delta H)}{\rho_c \cdot C_{pc}}$$

$$A9 = \frac{a_v \cdot \alpha_{fc}}{\rho_c \cdot C_{pc}}, \quad A10 = \frac{2 \cdot \alpha_{cw}}{R \cdot \rho_c \cdot C_{pc}}.$$

3.1.2. Characteristics of the model equations

The specific outer surface area of the catalyst pellets (a_v, m^2/m^3 cat) obtained experimentally appears in the above equations, so as to guarantee the mass and heat transfer terms consistent for the gas and solid phases. In the model equations used by Liu [6–8], Gilles [9] and Eigenberger [10,11], the specific outer surface area of catalyst bed (a'_v, m^2/m^3 bed) and specific outer surface area of a sphere ($3/R_p$, R_p is the radius of the catalyst pellets) are used at the same time. We do not think it is feasible. Not only confusion will arise, but also it is right coincidentally when $a'_v = 3(1-\epsilon)/R_p$.

Another feature of this model is that the heat transfer between the gas phase and the reactor wall, and the heat transfer between the particle phase and the wall are taken into consideration, respectively. The effective axial dispersion of the two phases are also taken into consideration in the model since the effective axial diffusivity is used to replace the molecular diffusivity.

3.2. Boundary and initial conditions

Different to our previous research [21], the so-called Danckwerts' boundary conditions are adopted in this work.

Boundary conditions are:

$$-D_{ea}\left.\frac{\partial C_f}{\partial X}\right|_{x=0} = U(C_0 - C_f), \quad \left.\frac{\partial C_f}{\partial X}\right|_{(X=L)} = 0, \quad (5)$$

$$-\lambda_f\left.\frac{\partial T_f}{\partial X}\right|_{x=0} = \rho_f U C_{pf}(T_0 - T_f), \quad \left.\frac{\partial T_f}{\partial X}\right|_{(X=L)} = 0, \quad (6)$$

$$-\lambda_{ea}\left.\frac{\partial T_c}{\partial X}\right|_{x=0} = \alpha_{fc} a_v (T_0 - T_c), \quad \left.\frac{\partial T_c}{\partial X}\right|_{(X=L)} = 0. \quad (7)$$

Initial conditions are:

$$C_f|_{(t=0)} = 0, \quad T_f|_{(t=0)} = T_{f0}, \quad C_c|_{(t=0)} = 0, \quad T_c|_{(t=0)} = T_{c0}. \quad (8)$$

4. Solution of the model equations

Since the inlet gas is at room temperature, and the oxidation of SO_2 is a strong exothermic chemical reaction, the axial temperature and concentration gradients in the flow-reversal fixed-bed reactor are very steep with their profiles varying with time.

There are three kinds of numerical methods for solving differential equations. For the orthogonal

collocation method which has been widely used in chemical engineering, sometimes a computer program based on this numerical method can be carried out quickly. But the collocation points are determined by the selected collocation functions, which cannot vary with the necessity in real circumstances, e.g., the distribution of physical variables. As the order of fit increases, the fit becomes sensitive to "noise", and results in instability [12]. For the finite difference method based on uniform grid, the computing time needed is comparatively long [13]. For the finite element method which has been applied to solve problems with irregular boundaries, it is difficult to treat this kind of unsteady-state problems with steep profiles of physical variables due to the strong exothermic chemical reaction. Thus the finite difference method with non-equidistance steps in space should be used. In the region where the gradient of the physical variables is large, the space step should be refined, otherwise, it could be enlarged. Though the total number of nodes used is the same, the values near the peak can be solved more accurately by adopting regional fine grid.

For the conventional finite difference method with non-equidistance spatial steps, the spatial steps change suddenly at the interface of the two regions with different spatial steps. Therefore, the accuracy at interface is low. Eigenberger [5] used a finite difference scheme to solve the one-dimensional pseudo-homogeneous unsteady-state model for a fixed-bed reactor. The scheme is of high-order accuracy on uniform grid. But due to the adoption of non-uniform spatial grid, the accuracy is lowered. The so-called "sag effects" [5] will emerge sometimes in numerical computations. Actually this phenomenon will appear in most of high-order schemes.

Here a Crank–Nicolson predictor–corrector finite difference method on the non-uniform spatial grid, which was devised tentatively in [21], is used to solve the derived partial differential equations. The prime feature is that the numerical method is of the second-order accuracy both in space and in time. The spatial steps change gradually. The two-way linked list defined in programming language C is selected to store the temperature and concentration of each node in the grid for adapting the change of the node number. Thus the computation accuracy and speed are improved remarkably.

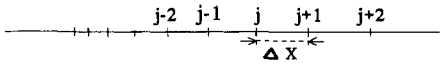

Fig. 2. Computational grid with spatial steps changing gradually.

4.1. Discretization of spatial derivatives

In Fig. 2, j denotes the coordinate of point X_j. By ordering $\Delta X_{j+1}-X_j$, and $\gamma_j = \Delta X_j/\Delta X_{j-1}$, and by using the Taylor series, the finite difference equations for the first and second-order derivatives of function $f(X)$ (f signifies an arbitrary function) at point X_j can be obtained.

$$\left.\frac{\partial f}{\partial X}\right|_j = \frac{f_{j+1} + (\gamma_j^2 - 1)\cdot f_j - \gamma_j^2 \cdot f_{j-1}}{\Delta X_j \cdot (1+\gamma_j)} - \frac{\Delta X_j \cdot \Delta X_{j-1}}{6} \cdot \left.\frac{\partial^3 f}{\partial X^3}\right|_j + O(\Delta X_j^3), \tag{9}$$

$$\left.\frac{\partial^2 f}{\partial X^2}\right|_j = \frac{f_{j+1} - (\gamma_j + 1)\cdot f_j + \gamma_j \cdot f_{j-1}}{(\Delta X_j \cdot \Delta X_{j-1} \cdot \gamma_{j+1})/2} - \frac{\Delta X_j - \Delta X_{j-1}}{3} \cdot \left.\frac{\partial^3 f}{\partial X^3}\right|_j + O(\Delta X_j^3). \tag{10}$$

In numerical computations, we choose $\Delta X_j = (1+\alpha\Delta X_{j-1})\Delta X_{j-1}$, where α is a bounded constant. Therefore, $\Delta X_j - \Delta X_{j-1} = \alpha\Delta X_{j-1}^2 = O(\Delta X_{j-1}^2)$, $\Delta X_j \Delta X_{j-1} = \Delta X_{j-1}^2 + \alpha\Delta X_{j-1}^3 = O(\Delta X_{j-1}^2)$. Hence, this scheme is of the second-order accuracy in space.

4.2. Discretization of time derivatives

Because the chemical reaction term introduces strong non-linearity, while the four partial differential equations are strongly coupled, the application of explicit scheme is restricted. For the conventional implicit scheme, the iterative operation is needed. Thus the amount of computation is great. The predictor–corrector method which has been used previously to simulate fixed-bed reactor with strong exothermic chemical reactions has the advantages of accuracy and efficiency [13]. Thus it is used again in this investigation. The first step is a semi-implicit scheme, while the second step is the Crank–Nicolson implicit scheme. This method which consists of two steps is of the second-order accuracy in the time direction, but the iterative operation is not needed.

4.3. Finite difference equations for the model equations

The four finite difference equations obtained by discretizing the four partial differential equations are given as follows:

Predictor (semi-implicit difference) scheme

$$\frac{C_f^{n+1/2}{}_j - C_{fj}^n}{\Delta t/2} + U_j^n \cdot \frac{C_f^{n+1/2}{}_{j+1} + (\gamma_j^2 - 1)\cdot C_f^{n+1/2}{}_j - \gamma_j^2 \cdot C_f^{n+1/2}{}_{j-1}}{\Delta X_j \cdot (1+\gamma_j)} = A1 \cdot \frac{C_f^{n+1/2}{}_{j+1} - (\gamma_j+1)\cdot C_f^{n+1/2}{}_j + \gamma_j \cdot C_f^{n+1/2}{}_{j-1}}{(\Delta X_j \cdot \Delta X_{j-1} \cdot \gamma_{j+1})/2} + A2 \cdot (C_c - C_f)_j^n. \quad (11)$$

$$\frac{T_f^{n+1/2}{}_j - T_{fj}^n}{\Delta t/2} + U_j^n \cdot \frac{T_f^{n+1/2}{}_{j+1} + (\gamma_j^2 - 1)\cdot T_f^{n+1/2}{}_j - \gamma_j^2 \cdot T_f^{n+1/2}{}_{j-1}}{\Delta X_j \cdot (1+\gamma_j)} = A3 \cdot \frac{T_f^{n+1/2}{}_{j+1} - (\gamma_j+1)\cdot T_f^{n+1/2}{}_j + \gamma_j \cdot T_f^{n+1/2}{}_{j-1}}{(\Delta X_j \cdot \Delta X_{j-1} \cdot \gamma_{j+1})/2} + A4 \cdot (T_c - T_f)_j^n + A5 \cdot (T_w - T_f)_j^{n+1/2}. \quad (12)$$

$$\frac{C_c^{n+1/2}{}_j - C_{cj}^n}{\Delta t/2} = A6 \cdot (C_f - C_c)_j^{n+1/2} - r(C_c, T_c)_j^n. \quad (13)$$

$$\frac{T_c^{n+1/2}{}_j - T_{cj}^n}{\Delta t/2} = A7 \cdot \frac{T_c^{n+1/2}{}_{j+1} - (\gamma_j+1)\cdot T_c^{n+1/2}{}_j + \gamma_j \cdot T_c^{n+1/2}{}_{j-1}}{(\Delta X_j \cdot \Delta X_{j-1} \cdot \gamma_{j+1})/2} + A8 \cdot r(C_c, T_c)_j^n + A9 \cdot (T_f - T_c)_j^{n+1/2} + A10 \cdot (T_w - T_c)_j^{n+1/2}. \quad (14)$$

Corrector (Crank–Nicolson implicit difference) scheme

$$\frac{C_f^{n+1}{}_j - C_{fj}^n}{\Delta t} + U_j^n \cdot \frac{C_f^{n+1}{}_{j+1} + (\gamma_j^2 - 1)\cdot C_f^{n+1}{}_j - \gamma_j^2 \cdot C_f^{n+1}{}_{j-1}}{2\cdot \Delta X_j \cdot (1+\gamma_j)} + U_j^n \cdot \frac{C_{fj+1}^n + (\gamma_j^2 - 1)\cdot C_{fj}^n - \gamma_j^2 \cdot C_{fj-1}^n}{2\cdot \Delta X_j \cdot (1+\gamma_j)} = A1 \cdot \frac{C_f^{n+1}{}_{j+1} - (\gamma_j+1)\cdot C_f^{n+1}{}_j + \gamma_j \cdot C_f^{n+1}{}_{j-1}}{\Delta X_j \cdot \Delta X_{j-1} \cdot \gamma_{j+1}} + A1 \cdot \frac{C_{fj+1}^n - (\gamma_j+1)\cdot C_{fj}^n + \gamma_j \cdot C_{fj-1}^n}{\Delta X_j \cdot \Delta X_{j-1} \cdot \gamma_{j+1}} + A2 \cdot (C_c - C_f)_j^{n+1/2}. \quad (15)$$

$$\frac{T_f^{n+1}{}_j - T_{fj}^n}{\Delta t} + U_j^n \cdot \frac{T_f^{n+1}{}_{j+1} + (\gamma_j^2 - 1)\cdot T_f^{n+1}{}_j - \gamma_j^2 \cdot T_f^{n+1}{}_{j-1}}{2\cdot \Delta X_j \cdot (1+\gamma_j)} + U_j^n \cdot \frac{T_{fj+1}^n + (\gamma_j^2 - 1)\cdot T_{fj}^n - \gamma_j^2 \cdot T_{fj-1}^n}{2\cdot \Delta X_j \cdot (1+\gamma_j)} = A3 \cdot \frac{T_f^{n+1}{}_{j+1} - (\gamma_j+1)\cdot T_f^{n+1}{}_j + \gamma_j \cdot T_f^{n+1}{}_{j-1}}{\Delta X_j \cdot \Delta X_{j-1} \cdot \gamma_{j+1}} + A3 \cdot \frac{T_{fj+1}^n - (\gamma_j+1)\cdot T_{fj}^n + \gamma_j \cdot T_{fj-1}^n}{\Delta X_j \cdot \Delta X_{j-1} \cdot \gamma_{j+1}} + A4 \cdot (T_c - T_f)_j^{n+1/2} + \frac{A5}{2} \cdot (T_w - T_f)_j^{n+1} + \frac{A5}{2} \cdot (T_w - T_f)_j^n. \quad (16)$$

$$\frac{C_c^{n+1}{}_j - C_{cj}^n}{\Delta t} = \frac{A6}{2} \cdot (C_f - C_c)_j^{n+1} + \frac{A6}{2} \cdot (C_f - C_c)_j^n - r(C_c, T_c)_j^{n+1/2}. \quad (17)$$

$$\frac{T_c^{n+1}{}_j - T_{cj}^n}{\Delta t} = A7 \cdot \frac{T_c^{n+1}{}_{j+1} - (\gamma_j+1)\cdot T_c^{n+1}{}_j + \gamma_j \cdot T_c^{n+1}{}_{j-1}}{\Delta X_j \cdot \Delta X_{j-1} \cdot \gamma_{j+1}} + A7 \cdot \frac{T_{cj+1}^n - (\gamma_j+1)\cdot T_{cj}^n + \gamma_j \cdot T_{cj-1}^n}{\Delta X_j \cdot \Delta X_{j-1} \cdot \gamma_{j+1}} + A8 \cdot r(C_c, T_c)_j^{n+1/2} + \frac{A9}{2} \cdot (T_f - T_c)_j^{n+1} + \frac{A9}{2} \cdot (T_f - T_c)_j^n + \frac{A10}{2} \cdot (T_w - T_c)_j^{n+1} + \frac{A10}{2} (T_w - T_c)_j^n. \quad (18)$$

4.4. Discretization of boundary conditions

The boundary condition is introduced by using the "reflection method" [12] which is also discussed in [13].

4.5. Modification of computational grids

4.5.1. Stability analysis of the difference scheme

Eqs. (1) and (2) belong to the convection–diffusion equation. When the axial effective mass diffusivity or thermal conductivity approaches zero, these equations change to the convection type. The convective numerical instability will take place while using our difference scheme (Eq. (9)). Fortunately, however, this phenomenon will not occur in the operation conditions of commercial plants. First, we define the grid Peclet number for temperature and concentration equation

$$Pe_T = \frac{C_{pf}\rho_f U \Delta X}{\lambda_{eg}}, \quad Pe_C = \frac{U\Delta X}{D_{ea}}. \tag{19}$$

It was found in numerical computations that when Pe_T>6, instability occurred in gas phase temperature equation, and when Pe_C>98, so did the gas phase concentration equation. Patankar [14] recommended to use the central difference scheme when Pe_T<2. When the actual gas velocity (U) is 0.3 m/s, the spatial step (ΔX) is 0.01 m, Pe_T is 0.15, Pe_C is 3.3. Thus our numerical scheme can be used in the operation conditions of commercial plants.

4.5.2. Spatial step and time step

The maximum spatial step should be small enough to ensure Pe_T less than 2. The minimum spatial step should not be too small in order to increase computation speed. Though the Crank–Nicolson scheme is absolutely stable, the time step should be less than $\Delta X^2/U$ according to our experience. In the first stage of numerical computation, the time steps should be even small to suppress instability which occurs in the initial stage of computation while using the Crank–Nicolson scheme.

4.5.3. Modification of spatial grid

Because the variation of the profile of T_f, T_c, C_f, or C_c is similar, the computational grid is modified according to the distribution of gas temperature (T_f). When the gas temperature difference between the nearby nodes exceeds a certain value, the computational grid is refined, otherwise, it is loosened. When the grid is changed, the values on new nodes are interpolated by the third-order spline function. In order to avoid frequent modification of the computational grid, a modification should be suitable and sufficient, i.e., to guarantee that a certain number of nodes are densely allocated immediately ahead of the heat front.

4.6. Solution of the algebraic equations

The coefficient matrices of the derived algebraic equations of both predictor and corrector steps are tri-diagonal matrices wherein the diagonal values are predominant. Therefore, the tri-diagonal matrix algorithm [13] can be employed.

4.7. The storage method for the numerical data

The storage method for the temperature or concentration of the gas or particle phase belongs to the problem of data structure of computer software engineering. With the traditional data structure, array, the designated dimension of the array cannot be changed when it is necessary. It is also cumbersome to insert a new node or delete a redundant one. It is desired to define a data structure with changeable dimension for efficient utilization of hardware resources. The so-called dynamic data structure can solve this problem. In this investigation the two-way linked list is adopted.

5. Results and discussion

5.1. A numerical example

A 28 mm i.d. flow-reversal fixed-bed reactor [15], with a length of 1100 mm, is employed. There is a layer of ϕ 5 mm bead placed below and atop the active catalyst section [15]. The rate equation of SO_2 oxidation is given in Ref. [16]:

$$r(SO_2) = \frac{K_{1,0}\cdot\exp(-E_1/R_gT)\cdot P_{SO_2}\cdot P_{O_2}^m\cdot(1-\beta)}{P_{SO_2}+K_{2,0}\cdot\exp(E_2/R_gT)\cdot P_{O_2}^m + K_{3,0}\cdot\exp(E_3/R_gT)\cdot P_{SO_3}}, \tag{20}$$

where $K_{i,0}$, m and E_i, (i=1,2,3) are listed in Table 1.

The axial effective thermal conductivity of the solid phase [17] is given by

Table 1
Parameters for SO_2 oxidation in a flow-reversal fixed-bed reactor

Parameters	643–713 K	713–823 K
Reaction		
Frequency factor (s^{-1})	$K_{1,0}=9.31\times10^5$	$K_{1,0}=18.12$
	$K_{2,0}=0$	$K_{2,0}=1.84\times10^{-5}$
	$K_{3,0}=0$	$K_{3,0}=2.89\times10^4$
Activation energy (J/mol)	$E_1=148\,565$	$E_1=78\,090$
	$E_2=0$	$E_2=55\,588$
	$E_3=0$	$E_3=-68\,772$
Reaction order of O_2	$m=0.5$	$m=0.63$
Heat of reaction	$-\Delta H=96\,232$ J/mol	
Catalyst		
Heat capacity of particle	$C_{pc}=876.5$ J/m^3 K	
Density of particle	$\rho_c=1150$ kg/m^3	
Radius of particle pellets	$R_p=0.006$ m	
Specific outer surface area	$a_v=410$ m^{-1}	
Reactor		
Length	$L=1.1$ m	
Radius	$R=0.014$ m	
Bed void fraction	$\epsilon=0.4$	
Interstitial gas velocity	$U=0.2$ m/s	
Wall temperature	$T_w=310$ K	
Heat capacity of gas	$C_{pf}=728.3$ J/m^3 K	
Density of gas	$\rho_f=1.384$ kg/m^3	
Feed concentration	$C_{f0}=3$ mol/m^3	
Initial bed temperature	$T_{c0}=720$ K	
Feed temperature	$T_{f0}=350$ K	

$$\lambda_{ec} = \lambda_f \cdot (7.9 + 0.8 \cdot Pr \cdot Re) \quad (21)$$

and λ_{ef} is considered, as by Eigenberger, to be equal to λ_{ec}. λ_f is the thermal conductivity of gas.

$$\lambda_f = 5.6 \times 10^{-5} T_f + 0.0111. \quad (22)$$

The axial effective mass diffusivity of gas phase [17] is given by:

When $Re<1$

$$D_{ea} = \frac{E^0}{\epsilon}. \quad (23)$$

When $Re>5$

$$D_{ea} = \frac{E^0}{\epsilon_b} + 0.5 D_p U, \quad (24)$$

where

$$\frac{E^0}{\mu_f} = (0.6 - 0.8)\epsilon_b. \quad (25)$$

Here 0.8 is chosen. μ_f is the mass diffusivity of gas,

$$\mu_f = 3.44 \times 10^{-8} T_f + 8.86 \times 10^{-6}. \quad (26)$$

In this investigation, the reactor wall is assumed as adiabatic.

$$\alpha_{fw} = \alpha_{pw} = 0.$$

The gas–particle mass transfer coefficient (β) [18,19] is given by

$$j_D = \frac{\beta}{U} Sc^{2/3} = \frac{0.725}{Re^{0.41} - 0.15}, \quad (27)$$

where $Sc = \mu_f / D_{ea} \rho_f$.

The gas–particle heat transfer coefficient (α_{fc}) is obtained from the correlation j-factors [18,19].

$$j_H = \frac{\alpha_{fc}}{(\rho C_p)_f} U Pr^{2/3} = j_D / 0.66, \quad (28)$$

where $Pr = C_{pf}\mu_f / \lambda_f$

5.2. Parameter sensitivity

The parameter sensitivity is carried out carefully for the mathematical model. The influences of the axial effective thermal conductivity of the two phases, and the axial effective mass diffusivity of the gas phase, etc. on the temperature and concentration profiles are studied.

To get a feeling for the importance of the axial effective thermal conductivity of the gas or solid phase, numerical simulation was performed with values of λ_{ef} and λ_{ec} about 10% higher than those calculated from Eq. (21). It was found that the temperature profile was changed, the creeping velocity was reduced and the cycle time was increased. Therefore, the model is sensitive to the axial effective thermal conductivity.

When 0.6 was chosen for Eq. (25), the influence on calculated temperature and concentration profiles was completely negligible. Hence the mathematical model is insensitive to the axial mass diffusivity.

5.3. Start-up characteristics

Fig. 3 illustrates the transient gas temperature profiles. Initially the bed temperature is 720 K. The inlet gas is fed into the bed at room temperature. At the region near the entrance, the cold inlet gas is preheated by hot particles and the gas temperature rises. When the gas temperature rises to a certain value (ignition temperature), chemical reaction takes place, the temperature rises violently, and SO_2 concentration decreases rapidly in very short distance. Therefore, a temperature peak emerges. The gas temperature may be much higher than the particle temperature near the hot spot. Because the inlet gas is cold, the temperature of the particles at the region near the entrance decreases and the temperature peak creeps forward. When the temperature peak moves near the exit, the cold inlet gas is fed in from the other end of the reactor tube (which was the exit previously), so that the temperature peak moves in the reverse direction. At this time, the cold gas is heated by the hot particles near the entrance, while the cold particles near the exit are heated by the hot gas.

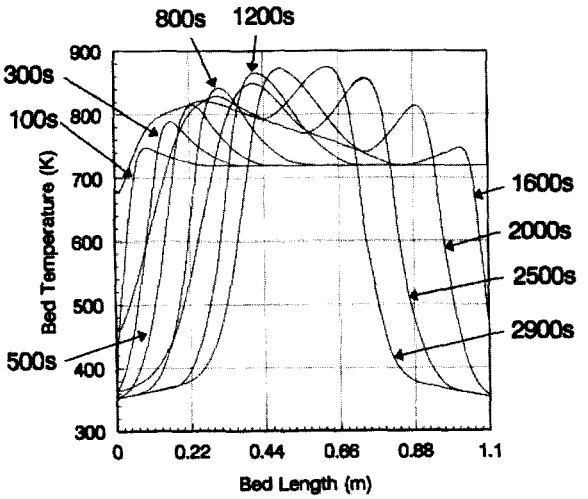

Fig. 3. Transient gas temperature profiles (L=1.1 m, U=0.3 m/s, T_{c0}=720 K, T_0=350 K, C_0=3 mol/m^3, T=3000 s).

5.4. Thermodynamic advantages

The thermodynamic advantages of the fixed-bed catalytic reactor with periodic flow-reversal operation are as follows:

1. The cold inlet gas is heated by the hot solid near the entrance. Therefore, the heat exchanger for preheating cold inlet gas is not necessary. Because the inlet gas is cold, the maximum temperature may be much lower than that of the traditional fixed-bed reactor, thus interstage heat exchanger is also eliminated. The particles near the exit with relatively low temperature are heated by the hot gas, therefore, the gas leaving the reactor is not very hot, and it may be sent to the absorber without being cooled.
2. In the traditional fixed-bed reactor, the temperature at the hind part of the reactor is very high, which is harmful to reversible chemical reactions, e.g. the SO_3 will decompose in high temperature. In the fixed-bed reactor with flow-reversal operation, the gas temperature near the exit is lower than that of the center. Therefore, as the gas flows forward, whose temperature drops gradually, the oxidation of the remaining SO_2 takes place also.

5.5. Comparison of the simulated results with experimental data

Experimental conditions are: feed concentration is 2.63–9.5%, superficial gas velocity is 0.2 m/s, and

Table 2
Comparison of simulated results with experimental data

Feed concentration (%)	Cycle time (min)	Hot spot temperature (K)		Conversion (%)	
		Experimental	Numerical	Experimental	Numerical
9.50	70	843	829	96.0–98.1	97.2
5.88	70	813	815	96.7–97.9	97.6
4.50	30	818	806	96.5–98.2	97.8
2.63	30	778	811	97.5–99.0	98.0

cycle time is 30 or 70 min. The comparison of simulated results with experimental data [15] is listed in Table 2.

5.6. *Influences of design and operational parameters*

The influences of design and operational parameters on hot spot temperature, average conversion or cycle time are discussed below.

5.6.1. *Influences of bed length*

The influences of bed length on hot spot temperature and average conversion are illustrated in Fig. 4. It can be seen that the average conversion increases along with the increase of bed length. But when the bed length is greater than 6 m, it has little influence on the average conversion. The hot spot temperature increases along with the decrease of bed length. So the bed length should be long enough to reduce the hot spot temperature. The cycle time is in direct proportion to the bed length. The catalyst particles at the two ends of the fixed bed serve as thermal-capacitor, therefore, inert-filler is recommended to fill the two ends of the reactor. Thus longer cycle time can be obtained, while the amount of catalyst can be reduced.

5.6.2. *Influences of gas velocity*

The influences of actual gas velocity on hot spot temperature and average conversion are illustrated in Fig. 5. When the actual gas velocity increases, the hot spot temperature increases, while the average conversion of SO_2 decreases obviously. The cycle time decreases obviously too. The reaction zone moves along with the gas flow direction. That is to say, the reaction zone is being blown out of the reactor gradually. The movement of reaction zone can be explained by axial conduction process of heat. The axial effective thermal conductivity is in direct proportion to gas velocity as shown in Eq. (21). When the gas velocity increases, the reaction zone has the tendency to move along with the flow direction. But

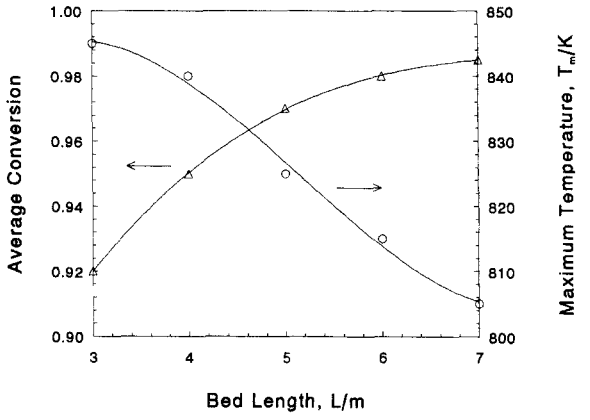

Fig. 4. Influences of bed length on hot spot temperature and average conversion (U=0.3 m/s, T_{c0}=720 K, T_0=350 K, C_0=2.5 mol/m^3, T=3600 s).

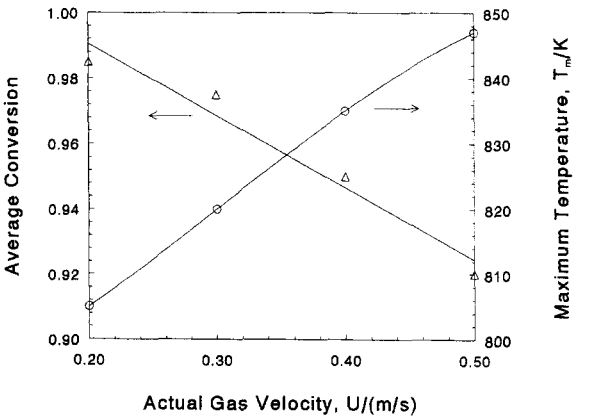

Fig. 5. Influences of actual gas velocity on hot spot temperature and average conversion (L=6.0 m, T_{c0}=720 K, T_0=350 K, C_0=2.5 mol/m^3, T=3600 s).

the axial effective thermal conductivity increases too, the reaction zone has the tendency to move against the flow direction because of the axial thermal dispersion. Therefore, the reaction zone moves slowly along with the flow direction. It is also found by numerical simulation that by adopting axial heat-conducting inserts, the axial effective thermal conductivity of the bed is 5–6-times that of before [13,20]. Therefore, the heat front creeps very slow along with the flow direction, and the cycle time can be comparatively long.

5.6.3. *Influences of initial bed temperature*

When the initial bed temperature is relatively low, almost no chemical reaction takes place. When the initial bed temperature exceeds a certain value, the ignition temperature, the oxidation will occur. It is found that when the initial bed temperature exceeds the ignition temperature, it has little effect on the average conversion, hot spot temperature, etc.

5.6.4. *Influences of feed concentration*

Fig. 6 shows the influences of feed concentration of SO_2 on hot spot temperature and average conversion. It can be seen that the average conversion decreases obviously with the increase of feed concentration, while the hot spot temperature increases.

5.6.5. *Influences of cycle time*

The influences of cycle time on hot spot temperature and average conversion are illustrated in Fig. 7.

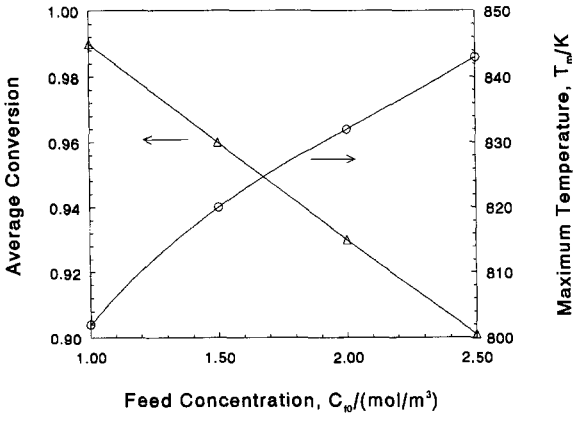

Fig. 6. Influences of feed concentration on hot spot temperature and average conversion (L=1.1 m, U=0.3 m/s, T_{c0}=720 K, T_0=350 K, T=3600 s).

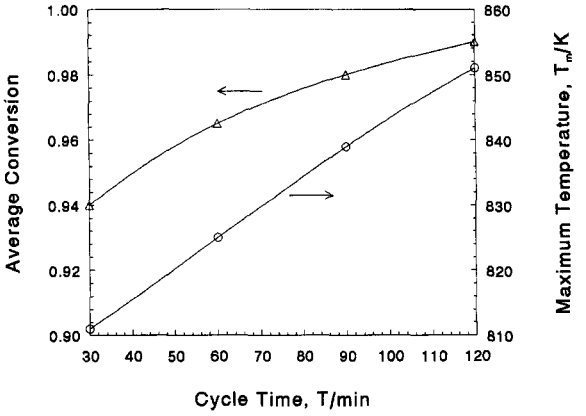

Fig. 7. Influences of cycle time on hot spot temperature and average conversion (L=1.1 m, U=0.3 m/s, T_{c0}=720 K, T_0=350 K, C_0=2.5 mol/m^3).

One may think that the average conversion will increase when the cycle time is reduced. Actually the average conversion and hot spot temperature decrease slightly when the cycle time is reduced. So it is recommended to employ longer cycle time if possible. But the cycle time should not be too long to extinguish the reactor.

6. Conclusions

1. The one-dimensional two-phase unsteady-state model for the oxidation of SO_2 in a fixed-bed catalytic reactor with periodic flow reversal is derived from the conservation of mass and heat. The boundary and initial conditions are obtained according to physical insight.
2. The predictor–corrector finite difference method based on the Crank–Nicolson scheme is used to solve the model equations on non-uniform grids. This scheme is of the second-order accuracy both in time and in space directions. It is comparatively efficient due to the exemption from iterative procedure. The dynamic data structure, two-way linked list is used in the computer program coded in language C to adapt the requirement of the algorithm. Thus, the computer program developed is more efficient.
3. The thermodynamic advantages of the fixed-bed reactor with periodic flow reversal are discussed.

4. It is found that the model is sensitive to the axial effective thermal conductivity of the two phases, and insensitive to axial effective mass diffusivity.
5. Influences of bed length, gas velocity of bed, initial bed temperature, feed concentration of SO_2, and cycle time on hot spot temperature and average conversion are obtained.

7. Notation

a_v	specific outer surface area of catalyst pellets, m^2/m^3 (cat)
C_f	concentration of SO_2 in the gas phase, mol/m^3 (gas)
C_c	concentration of SO_2 in the solid phase, mol/m^3
C_0	feed concentration of SO_2, mol/m^3
C_{pf}	heat capacity of gas, J/kg K
C_{pc}	heat capacity of solid, J/kg K
D_{ea}	axial effective diffusivity of gas, m^2/s
D_p	diameter of catalyst pellets=$2R_p$, m
L	length of the fixed-bed reactor, m
P	pressure, Pa
P_r	Prandtl number=$C_{pf}\mu_f/\lambda_f$
$r(SO_2)$	observed reaction rate, $kmol/m^3$ s
R_g	gas constant, 8.314 J/mol K
R	radius of fixed-bed reactor, m
Re	particle Reynolds number=$\rho_f U D_p/\mu$
R_p	radius of catalyst pellets, m
T	cycle time, s
T_0	inlet gas temperature, K
T_f	temperature of the gas phase, K
T_c	temperature of the solid phase, K
T_{f0}	initial gas temperature, K
T_{c0}	initial solid phase temperature, K
T_m	maximum gas phase temperature, K
t	time, s
U	actual gas velocity, m/s
X	axial coordinate, m

Greek letters

ρ_f	density of gas, kg/m^3
ρ_c	density of solid, kg/m^3
ϵ	voidage of catalyst bed
α_{fw}	gas–wall heat transfer coefficient, J/m^2 K s
α_{fc}	gas–solid heat transfer coefficient, J/m^2 K s
β	gas–solid mass transfer coefficient, m/s
$-\Delta H$	heat of reaction, J/mol
λ_f	thermal conductivity of gas, J/m K s
λ_{ef}	axial effective thermal conductivity of gas, J/m K s
λ_{ec}	axial effective thermal conductivity of solid, J/m K s

Subscripts

a	axial
c	catalyst phase
e	effective
g	gas phase
w	wall

Operators

$\nabla\cdot$	divergence
∇	gradient

Acknowledgements

This research was partially supported by CCAST (China Center of Advanced Science and Technology). The authors are also grateful to Prof. Dr. Zaisha Mao in preparation of this paper.

References

[1] Y.S. Matros, US Patent 4 478 808 (1984).
[2] Y.S. Matros, Unsteady Processes in Catalytic Reactors, Elsevier, Amsterdam, 1985.
[3] Y.S. Matros, G.A. Bunimovich, G.K. Boreskov, in: L.K. Doraiswamy, R.A. Mashelkar (Eds.), Frontiers in Chemical Reaction Engineering, vol. 2, 1984.
[4] G. Eigenberger and U. Nieken, Chem. Eng. Sci., 43 (1988) 2109.
[5] G. Eigenberger and J.B. Butt, Chem. Eng. Sci., 31 (1976) 681.
[6] S.L. Liu and N.R. Amundson, Ind. Eng. Chem. Fundam., 1 (1962) 200.
[7] S.L. Liu and N.R. Amundson, Ind. Eng. Chem. Fundam., 2 (1963) 12.

[8] S.L. Liu and N.R. Amundson, Ind. Eng. Chem. Fundam., 2 (1963) 183.
[9] E.D. Gilles, B. Luebeck, M. Zeitz, 4, IFAC Congress, Warschau, 1969, paper 46.2.
[10] G. Eigenberger, Chem. Eng. Sci., 27 (1972) 1909.
[11] G. Eigenberger, Chem. Eng. Sci., 27 (1972) 1917.
[12] P.J. Roache, Computational Fluid Dynamics, Hermosa Publishers, Albuquerque, NM, 1972.
[13] R. Hong, G. Xia, H. Li, W. Yuan, Analysis for ortho-dimethylbenzene oxidation in fixed bed using 2-D pseudo-homogeneous phase model, in: Proceedings of the 1996 Asian–Pacific Chemical Reaction Engineering Forum, June 1996, Beijing, China, p. 619.
[14] S.V. Patankar, Numerical heat transfer and fluid flow, Hemisphere, Washington, DC, 1980.
[15] W. Xiao, H. Xiang and W. Yuan, Sulfuric Acid Ind., 2 (1991) 13 (in Chinese).
[16] H. Guo, Z. Han and K. XieMechamsm and kinetics of SO_2 oxidation on "K–V" and "K–Na–V" catalyst series(II) kinetics, J. Chem. Ind. Engrg. (China), 3 (1984) 244 (in Chinese).
[17] N. Wakao, S. Kaguei, Heat and Mass Transfer in Packed Beds, Gordon and Breach, London, 1982.
[18] Wasch De A.P. and G.F. Froment, Chem. Eng. Sci., 26 (1971) 629–634.
[19] S. Li, Chemical and Catalyst Reaction Engineering, Chemical Industry Press, Beijing, 1986 (in Chinese).
[20] A. Walter and D. Vortmeyer, Ger. Chem. Eng., 3 (1980) 38.
[21] R. Hong, X. Li, H. Li, H. Li, W. Yuan, Mathematical modelling and numerical method of flow-reversal fixed bed, in: Proceedings of 1996 Asian–Pacific Chemical Reaction Engineering Forum, June 1996, Beijing, China, p. 657.